RMetS
Royal Meteorological Society

Weakly nonlinear Prandtl model for simple slope flows

Branko Grisogono,[a]* Toni Jurlina,[a] Željko Večenaj[a] and Ivan Güttler[b]
[a]*AMGI, Faculty of Science, Department of Geophysics, University of Zagreb, Croatia*
[b]*Meteorological and Hydrological Service (DHMZ), Zagreb, Croatia*

*Correspondence to: B. Grisogono, Department of Geophysics, Faculty of Science, University of Zagreb, Horvatovac 95, Zagreb 10000, Croatia. E-mail: bgrisog@gfz.hr

The Prandtl model couples, probably in the most succinct way, basic boundary-layer dynamics and thermodynamics for pure anabatic and katabatic flows over inclined surfaces by assuming a one-dimensional steady-state balance between buoyancy and turbulent friction. Although the classic Prandtl model is linear, having an a priori assigned vertically constant eddy diffusivity and heat conductivity, K, in this analytic work we partly relax both of these restrictions. The first restriction is loosened by using a weakly nonlinear approach where a small parameter, ε, controls feeding of the flow-induced potential temperature gradient back to the environmental potential temperature gradient, because the former, below the katabatic jet, can be 20–50 times stronger than the latter, background or free-flow gradient. An appropriate range of values for ε, controlling the weak nonlinearity for pure katabatic flow, is provided. In this way, the near-surface potential temperature gradient becomes stronger and the corresponding katabatic jet somewhat weaker (at a slightly lower height) than that in the classic Prandtl solution. The second restriction is partly relaxed by using a prescribed, gradually varying K with distance from the underlying surface, all within the usual validity of the zero-order Wentzel–Kramers–Brillouin approximation to solve the coupled differential equations. The new model is compared with the glacier wind data from the Pasterze experiment (PASTEX-94), Austria. Further discussion includes gradient Richardson number consideration and an application to simple anabatic flows. The model may be applied for estimation and interpretation of the wind affecting glacier mass balance and air pollution.

Key Words: anabatic and katabatic flow; glacier wind; inclined boundary layers; WKB method

Received 11 December 2013; Revised 8 April 2014; Accepted 26 May 2014; Published online in Wiley Online Library

1. Introduction

The theory, modelling and overall understanding of the very stably stratified atmospheric boundary layer (SABL) is still far from being complete (e.g. Mahrt, 1998; Grisogono and Oerlemans, 2001a; Mauritsen *et al.*, 2007; Rotach and Zardi, 2007; van de Wiel *et al.*, 2007; Belušić and Mahrt, 2008; Zilitinkevich *et al.*, 2008; Belušić and Güttler, 2010; Grisogono, 2010; Baklanov *et al.*, 2011). Based on the gradient Richardson number, Ri, i.e., the ratio of buoyancy frequency squared to wind shear squared, one of the types of the very SABL is pure katabatic flow, there $Ri \to \infty$ at the height of the low-level jet (LLJ). This jet appears in drainage type of flows with a speed of, say $\sim O(5\ \mathrm{m\ s^{-1}})$. It may even occur at a few or several metres above the underlying inclined cooled surface, thus often violating the Monin–Obukhov surface-layer scaling, as discussed by Mahrt (1998, 2008a, 2008b, 2014), Smeets *et al.* (1999), Van der Avoird and Duynkerke (1999), Grisogono *et al.* (2007), Fedorovich and Shapiro (2009) and Nadeau *et al.* (2013). Pure katabatic, thermally driven LLJ should not be confused with other types of LLJs, for instance, with a downslope wind due to, e.g., a mountain-lee windstorm (with a shooting flow), such as a strong bora wind (Smith, 1987; Grisogono and Belušić, 2009; Chow *et al.*, 2013).

The overall relevance and importance of near-surface drainage-type flows has been documented by, e.g., Oerlemans and Vugts (1993), Oerlemans *et al.* (1999) and also stated by Baklanov *et al.* (2011). Almost needless to say, katabatic and drainage flows are ubiquitous over mountainous and other complex terrain wherever underlying surface inclination exists over an appreciable distance (e.g. Nappo and Rao, 1987; Oerlemans, 2001; Renfrew and Anderson, 2002, 2006); hence, such flows modulate local and regional climate (e.g. van den Broeke and Lipzig, 2003), affect the mass balance of glaciers (e.g. Munro, 2004), affect sea-ice thinning and production (e.g. Barthélemy *et al.*, 2012) and play a role in wind-energy harvesting (e.g. Horvath *et al.*, 2011). However, those flows are often unresolved in both standard measurements and most operational models. Meanwhile, as numerical weather prediction (NWP) and climate models reach ever refined resolution, various flows over progressively more sloping terrain are simulated, but the related treatment of the lower boundary conditions, near-surface turbulence parametrization, etc., remain unsettled issues

(e.g. Mahrt, 1998, 2014; Epifanio, 2007; Grisogono *et al.*, 2007; Buzzi *et al.*, 2011; Chow *et al.*, 2013). Thus, katabatic as well as anabatic flows remain the subject of vigorous research (e.g. Princevac and Fernando, 2007; Fedorovich and Shapiro, 2009; Shapiro *et al.*, 2012; Zardi and Whiteman, 2013). All of which leads to the aim of this work.

There are various aspects, modifications and improvements to basic and advanced models of katabatic flows (e.g. Gutman, 1972; Mahrt, 1982; Nappo and Rao, 1987; Egger, 1990; Smith and Skyllingstad, 2005; Kavčič and Grisogono, 2007; Axelsen and van Dop, 2009a; Burkholder *et al.*, 2009; Zardi and Whiteman, 2013). With some valuable exceptions (e.g. Egger, 1990; Burkholder *et al.*, 2009; Shapiro *et al.*, 2012), most of the analytic katabatic models are one-dimensional models. Furthermore, one of the more common analytic models for the corresponding thermally driven simple slope flows is that of Prandtl (1942), as also referred to elsewhere (Defant, 1949; Lykosov and Gutman, 1972; Mahrt, 1982; Egger, 1990; Oerlemans, 2001; Axelsen and van Dop, 2009b). Advantages and weaknesses of the classic Prandtl model were recently discussed by Grisogono and Axelsen (2012), primarily in the light of large-eddy simulation (LES) and secondly, in terms of a limited observational data set (e.g. van den Broeke, 1997a, 1997b; Oerlemans and Grisogono, 2002; Parmhed *et al.*, 2004; Axelsen and van Dop, 2009a, 2009b). Further improvements in treating certain shortcomings of the classic Prandtl model are in Mo (2013). Overall, one of the main drawbacks for most analytic models of katabatic flows, including the classic Prandtl model, is the assumed linearity and prescribed constancy of eddy diffusivity and conductivity (all for the sake of mathematical tractability). The latter issue can often be at least partly treated via eddy diffusivity that varies gradually with height and using the WKB(J)* method (e.g. Bender and Orszag, 1978), as done for katabatic flows in Grisogono and Oerlemans (2001a, 2001b, 2002; hereafter GOa, GOb, GO2). In this way, the near-surface gradients of certain important meteorological fields become sharper and closer to the surface – the information that is typically missed by many operational NWPs, even research numerical models, not to mention climate models (e.g. Svensson and Holtslag, 2009; Nikulin *et al.*, 2011; Chow *et al.*, 2013). Besides turbulence parametrization and the mentioned eddy-diffusivity approach, the prime drawback of typical analytic models remains the presumed flow linearity.

Focusing on analytic models for katabatic flows, the principal weakness of such models, including the classic Prandtl model, is that the strong, near-surface flow-related finite-amplitude potential temperature gradient does not feed back onto the imposed environmental potential temperature gradient in the corresponding thermodynamic equation. In other words, even though the induced temperature gradient below the katabatic LLJ can be 20 to even 50 times stronger than the related environmental gradient (GOa; Oerlemans, 2001; Grisogono and Axelsen, 2012), the analytic near-surface katabatic wind does not sense quick temperature profile adjustment after the initial discontinuity in the potential temperature if the time evolution is also taken into account (e.g. Grisogono, 2003). It is proposed here that it is the induced rapid near-surface potential temperature gradient that should shape the consequent wind profile adjustment, and we shall address such an issue at its steady state. This proposal might also address the dependence of the maximum katabatic wind speed on the slope angle, which is not comprised in the linear Prandtl theory (Oerlemans and Grisogono, 2002; Grisogono and Axelsen, 2012). Of course, the whole process between the temperature and wind speed ought to be interactive, time-dependent and fully nonlinear; however, in an analytic treatment of an existent, simple but rather robust model, such as that of Prandtl, a step forward in improving it should bring further understanding of both the model and simple sloped flows as such. In this way, more is learnt about the model itself and eventually the model may come a step closer to reality.

The objective of this study is to introduce a single modification and eventual improvement to a linearly improved Prandtl model with gradually varying eddy diffusivity and conductivity (GOa, b; GO2) that has previously been used and evaluated (Parmhed *et al.*, 2004). Moreover, the mentioned gradual variability, within the WKB approach, has been deployed and validated in the context of SABL modelling elsewhere (Jeričević *et al.*, 2010, 2012). A weakly nonlinear form of the previously improved Prandtl model (GO2; Parmhed *et al.*, 2004) is assumed here, so that the strong near-surface potential temperature gradient, $\partial\theta/\partial z$, feeds back to the assigned background or free-flow potential temperature gradient Γ. Here we make a contribution by tackling a nonlinear improvement of the Prandtl model modified by (or 'immersed' in) gradually varying background eddy diffusivity and conductivity. While the focus is on simple katabatic flow, the same approach may be easily adjusted to simple anabatic flow. Section 2 presents development of the weakly nonlinear Prandtl model for simple katabatic flows. Section 3 provides data comparison, discussion and a digression for simple anabatic flow; finally, conclusions are summarized in section 4.

2. Weakly nonlinear Prandtl model

2.1. Zero-order solution

The classic Prandtl model has been presented and used in numerous publications over more than 70 years (Prandtl, 1942; Defant, 1949; Smith, 1979; Mahrt, 1982; Egger, 1990; GOa; Stiperski *et al.*, 2007; Axelsen and van Dop, 2009b), including its straightforward extension to slowly varying eddy coefficients (GOb; Parmhed *et al.*, 2004; Kavčič and Grisogono, 2007) during the past 13 years or so. Before we present the newly modified weakly nonlinear Prandtl model in the context of gradually varying background eddy coefficients, we want to mention that all the detailed derivations from the original Prandtl model throughout are given in Jurlina (2013).

The simplified governing steady-state one-dimensional equations in the tilted coordinate frame for a constant slope α, $|\alpha| \ll 1$ so that the quasi-hydrostatic approximation is valid (Mahrt, 1982; Haiden, 2003; Grisogono and Axelsen, 2012), are for the momentum and thermodynamics (e.g. Denby, 1999; Stiperski *et al.*, 2007), respectively:

$$\begin{aligned} 0 &= g\frac{\theta}{\Theta_0}\sin(\alpha) + KPr\frac{\partial^2 u}{\partial z^2} \\ 0 &= -\left(\Gamma + \varepsilon\underline{\frac{\partial\theta}{\partial z}}\right)u\sin(\alpha) + K\frac{\partial^2\theta}{\partial z^2}, \end{aligned} \tag{1}$$

where the new term is underlined and the symbols have their usual meaning including: g is acceleration due to gravity, θ is the potential temperature deviation from the background temperature Θ, K and Pr are eddy heat conductivity and turbulent Prandtl number (the latter assumed as a constant), u is the downslope (katabatic) wind component, z is the coordinate perpendicular to the constant slope surface, $\alpha < 0$ for katabatic and $\alpha > 0$ for anabatic flow (since $|\alpha| \ll 1$, this is not far away from true vertical in the very SABL, which is a relatively thin layer, say $\sim O$ (50 m), adjacent to the surface) and Θ_0 is a reference temperature. Hence, the free-flow Γ is defined in the true vertical coordinate frame (where the buoyancy acts) as $\Gamma \equiv \mathrm{d}\Theta/\mathrm{d}z^*$, where z^* is in the true vertical direction. Besides the assumed steady-state (thus, the local change on the left-hand side is 0) and one-dimensional slope flow without an imposed pressure gradient field, quasi-hydrostatic, Boussinesq and rotation-free approximations are included in the system (1). The only new term in Eq. (1), as underlined in the thermodynamic equation,

*After Wentzel, Kramers and Brillouin, who used and popularized the method in theoretical physics. Sometimes also referred to as WKBJ, including Jeffreys who, as Rayleigh, contributed to its early development. The original approximation was made independently by Green and Liouville in 1837.

modulates the amount of nonlinearity (presumably weak in terms of regular perturbation analysis) via small parameter ε, where $0 \leq \varepsilon \ll 1$. This term could have been derived more rigorously from a fuller original thermodynamic equation by expanding the meteorological fields and assuming the regular perturbation analysis (e.g. Bender and Orszag, 1978; Pedlosky, 1987) for the background windless conditions, but here it is more appealing in its heuristic appearance and the consequent modification of the meteorological fields (u, θ). The underlined term in Eq. (1) enhances the along-slope advection of θ that is counteracted by the parametrized turbulent mixing. Note that a qualitatively similar treatment of a sea breeze is presented by Gutman (1972); the wind speed there evolves linearly while the potential temperature behaves nonlinearly through an interaction with the wind speed.

The system (1) is invalid for $\alpha = 0$ because no complete tensor coordinate transformation is performed (e.g. Pielke, 1984); however, if Eq. (1) is extended so that it contains additional damping mechanisms, as in Mo (2013), this zero-slope singularity is removed. As we are interested here in slopes from, say, a half of a degree and more, the zero-slope issue is irrelevant here. For example, if $\Gamma = 3$ K km^{-1} and $\alpha = 0.5^\circ$, the characteristic time-scale for the katabatic flow development is over 19 h, which is too long for most katabatic winds out of the polar regions.

Once again, the only difference between Eq. (1) and the classic Prandtl model is the presence of the $\varepsilon \partial\theta/\partial z$ term, which is motivated by the fact that $\Gamma \ll \partial\theta/\partial z$ around and below the katabatic jet, z_j, i.e., for $z \leq z_j$, or $z \sim z_j$. At the same time, the regular perturbation analysis is perhaps the simplest and most powerful method to treat nonlinearity in this case. Moreover, the zero-order WKB approach can be directly applied here for the treatment of the gradually varying eddy conductivity $K(z)$ and diffusivity $K(z)Pr$ in Eq. (1) (GOa, b; Parmhed *et al.*, 2004). This means that Eq. (1), including its zero-order solutions, i.e., exponentially decaying functions of z, remains the same as in the classic Prandtl model, while the coefficients parametrizing turbulent exchange of momentum and heat become slowly varying functions of z, so that their derivatives do not affect the basic dynamics in Eq. (1) explicitly. However, local values of $K(z)$ are taken into account as integrals between the surface and actual elevation considered. For this to be valid, it must be satisfied that $h > z_j$, where h is the scale height for $K(z)$ (details in GOa, b; GO2). Furthermore, Pr also could have been made a gradually varying function; however, because relatively little is known about Pr variability in the SABL, Pr constancy is assumed here.

Next, we make a global expansion of (u, θ) into:

$$u_{\mathrm{tot}} = u_0 + \varepsilon u_1 + \varepsilon^2 u_2 + \dots$$
$$\theta_{\mathrm{tot}} = \theta_0 + \varepsilon \theta_1 + \varepsilon^2 \theta_2 + \dots, \qquad (2)$$

where the subscripts on the right-hand-side mean the zero-order flow variables (as in the classic Prandtl model), the first-order corrections (i.e. weakly nonlinear here), etc. We insert Eq. (2) into Eq. (1) and obtain an infinite set of two-equation systems in the order of powers of ε, i.e., ε^0, ε^1, etc. However, we keep this expansion only up to its first order for simplicity. The solution to ε^0 order is already known from numerous previous studies (e.g. Defant, 1949; Egger, 1990; GOa) and is given here for the overall readability. Nonetheless, it was not previously presented in the context of this perturbation expansion; it reads

$$u_0(z) = -C\mu \exp\left(-\frac{z}{h_{\mathrm{P}}}\right) \sin\left(\frac{z}{h_{\mathrm{P}}}\right)$$
$$\theta_0(z) = C \exp\left(-\frac{z}{h_{\mathrm{P}}}\right) \cos\left(\frac{z}{h_{\mathrm{P}}}\right), \qquad (3a)$$

where C is, in case of katabatic flows, the surface potential temperature deficit, $C < 0$ (the opposite is for anabatic flows with a temperature surplus), $\mu = [g/(\Theta_0 \Gamma Pr)]^{1/2}$ is a dimensional parameter, h_{P} is the characteristic depth of the Prandtl layer, $h_{\mathrm{P}} = \sqrt{2}/\sigma$, σ is the characteristic 'wave number', $\sigma = [N \sin(\alpha)/(KPr^{1/2})]^{1/2}$, N is the background or free-flow buoyancy frequency, $N^2 = \Gamma g/\Theta_0$ and K is an average eddy conductivity. The boundary conditions (BC) imposed are the usual ones for the Prandtl model: $\theta_{\mathrm{tot}}(z = 0) = C$, $u_{\mathrm{tot}}(z = 0) = 0$, $\theta_{\mathrm{tot}}(z \to \infty) = 0$, $u_{\mathrm{tot}}(z \to \infty) = 0$, where in the classic Prandtl model the subscript 'tot' trivially becomes 0. Note that $u_0(z)$ maximizes at $z_j = h_{\mathrm{P}}\pi/4$ within statically very strongly stratified conditions and below a typical but vaguely defined inversion top (e.g. Mahrt, 1998; GO2). To add a point, Stiperski *et al.* (2007) show that Eq. (3a) is a valid solution to the Prandtl model even for finite-amplitude simple slope flows.

Within the zero-order WKB approach, pertaining to the so-called solution's controlling behaviour, system (1) can be transformed to a single governing equation of the fourth order for (u, θ), representing in both cases a heavily damped oscillator (e.g. Grisogono, 2003):

$$\frac{\mathrm{d}^4(u,\theta)}{\mathrm{d}z^4} + N^2 \frac{\sin^2(\alpha)}{PrK(z)^2}(u,\theta) = 0,$$

where $K(z)$ is a gradually varying part of the non-constant overall 'coefficient' in the second term. Hence, the argument in Eq. (3a), z/h_{P}, becomes a simple integral, i.e., $z/h_{\mathrm{P}} \to \int \mathrm{d}z/h_{\mathrm{P}} = I(z)$, where the arrow indicates the transformation from the variable of constant-coefficient differential equation to the WKB-type variable of gradually varying-coefficient differential equation. In this way, $I(z)$ is

$$I(z) = \left(\frac{\sigma_0}{2}\right)^{\frac{1}{2}} \int_0^z K(z)^{-\frac{1}{2}} \mathrm{d}z,$$

with $\sigma_0^{1/2}$ as the factor in $I(z)$, $\sigma_0 = [N \sin(\alpha) Pr^{-1/2}]$; thus, Eq. (3a) generalizes to

$$u_{0,\mathrm{WKB}}(z) = -C\mu \exp[-I(z)] \sin[I(z)],$$
$$\theta_{0,\mathrm{WKB}}(z) = C \exp[-I(z)] \cos[I(z)], \qquad (3b)$$

of course, the lower integration limit for $I(z)$ might go from the roughness height, z_0, upward, but this is not crucial here. The details of the WKB method, which belongs to global singular perturbation methods, applied to the Ekman or Prandtl model are elaborated by Berger and Grisogono (1998), GOa, GO2 and the consequent articles. The main point with the WKB approximation here is that in Eq. (3b) the argument under the exponential and trigonometric functions becomes the integral $I(z)$, and the solutions are no longer strictly periodic functions. Moreover, the simplicity and the elegance of the basic, classic solution of Prandtl for $K = \mathrm{const}$, Eq. (3a), is clearly retained in Eq. (3b).

2.2. *First-order correction*

Next, we analyse the first-order corrections to Eq. (1) while invoking the zero-order WKB method[†] (e.g. Bender and Orszag, 1978). The corresponding system at the order of ε^1, with (or similarly without) the WKB approximation, is

$$0 = g\frac{\theta_{1,\mathrm{WKB}}}{\Theta_0} \sin(\alpha) + KPr \frac{d^2 u_{1,\mathrm{WKB}}}{\mathrm{d}z^2}$$
$$0 = -\left(\Gamma u_{1,\mathrm{WKB}} + \frac{d\theta_{0,\mathrm{WKB}}}{\mathrm{d}z} u_{0,\mathrm{WKB}}\right) \sin(\alpha) + K \frac{d^2 \theta_{1,\mathrm{WKB}}}{\mathrm{d}z^2}, \qquad (4)$$

[†]If a higher order WKB approximation was to be included, it would be necessary to expand the equations and solutions in terms of yet another small parameter, say δ, and to group the terms with the alike power of δ and solve the consequent equations. The solutions should be proportional to $\exp[(S_0 + \delta S_1 + \delta^2 S_2 + \dots)/\delta]$; the zero-order WKB solution is associated with the S_0 term in this expansion.

where the unknowns are $(u_{1,\mathrm{WKB}},\ \theta_{1,\mathrm{WKB}})$ and the forcing is provided by the zero-order field, $(u_0,\ \theta_0)$, represented by the second term in the parentheses of the second equation in Eq. (4). After arranging the terms, Eq. (4) again yields the damped oscillator equation but now with the different forcing on the corresponding right-hand sides for $u_{1,\mathrm{WKB}}$ and $\theta_{1,\mathrm{WKB}}$:

$$\frac{\mathrm{d}^4\theta_{1,\mathrm{WKB}}}{\mathrm{d}z^4}+N^2\frac{\sin^2(\alpha)}{PrK(z)^2}\theta_{1,\mathrm{WKB}}=\frac{\sin(\alpha)}{K(z)}\frac{d^2}{\mathrm{d}z^2}\left(u_{0,\mathrm{WKB}}\frac{\mathrm{d}\theta_{0,\mathrm{WKB}}}{\mathrm{d}z}\right),$$
$$\frac{\mathrm{d}^4u_{1,\mathrm{WKB}}}{\mathrm{d}z^4}+N^2\frac{\sin^2(\alpha)}{PrK(z)^2}u_{1,\mathrm{WKB}}=-\frac{g\sin^2(\alpha)}{\Theta_0K(z)^2Pr}u_{0,\mathrm{WKB}}\frac{\mathrm{d}\theta_{0,\mathrm{WKB}}}{\mathrm{d}z}. \tag{5}$$

We impose the following BCs to the inhomogeneous ordinary differential equations (5): $\theta_{1,\mathrm{WKB}}(0)=0$, $u_{1,\mathrm{WKB}}(0)=0$, $\theta_{1,\mathrm{WKB}}(z\to\infty)=0$, $u_{1,\mathrm{WKB}}(z\to\infty)=0$. Qualitatively speaking, for $\alpha<0$, as considered for katabatic flows here, the right-hand-side forcing of the $(u_{1,\mathrm{WKB}},\theta_{1,\mathrm{WKB}})$ correction implies a mostly positive contribution for $\theta_{1,\mathrm{WKB}}$ and a mostly negative one for $u_{1,\mathrm{WKB}}$ (with the opposite effect for anabatic flows). It is noteworthy that Eq. (5) is one of novelties of this study; it has significant consequences for the dynamics of slope flows.

After a lengthy but straightforward calculation, assuming that the solutions $(u_{1,\mathrm{WKB}},\theta_{1,\mathrm{WKB}})$ resemble the zero-order solutions in Eq. (3b), which is due to the nature of the imposed forcing in Eq. (5), the following is obtained:

$$\begin{aligned}\theta_{1,\mathrm{WKB}}(z)&=\theta_{\mathrm{A,WKB}}\exp[-I(z)]\\&\times\left\{-\frac{1}{15}\sin[I(z)]-\frac{1}{6}\cos[I(z)]\right\}+\theta_{\mathrm{A,WKB}}\exp[-2I(z)]\\&\times\left\{\frac{1}{15}\sin[2I(z)]+\frac{1}{15}\cos[2I(z)]+\frac{1}{10}\right\},\\u_{1,\mathrm{WKB}}(z)&=u_{\mathrm{A,WKB}}\exp[-I(z)]\\&\times\left\{-\frac{1}{3}\sin[I(z)]+\frac{2}{15}\cos[I(z)]\right\}+u_{\mathrm{A,WKB}}\exp[-2I(z)]\\&\times\left\{\frac{1}{30}\sin[2I(z)]-\frac{1}{30}\cos[2I(z)]-\frac{1}{10}\right\},\end{aligned} \tag{6a}$$

where the (previously strictly constant) amplitudes are now:

$$\theta_{\mathrm{A,WKB}}=\left(\frac{2}{\sigma_0}\right)^{\frac{1}{2}}C^2\mu\sin(\alpha)K(z)^{-\frac{1}{2}},$$

and

$$u_{\mathrm{A,WKB}}=\left(\frac{\sigma_0}{2}\right)^{\frac{1}{2}}C^2\frac{\mu}{\Gamma}K(z)^{-\frac{1}{2}}, \tag{6b}$$

with subscript A for both corresponding gradually varying amplitudes in $(u_{1,\mathrm{WKB}},\ \theta_{1,\mathrm{WKB}})$, and $I(z)$ remains the same as before. The correction amplitudes in Eq. (6b) vary gradually because of $K(z)$, where a small minimum value, say $\sim 10^{-4}\mathrm{m}^2\ \mathrm{s}^{-1}$, prevents a possible division by 0 (see section 2.4). More importantly, all the terms added within the braces of Eq. (6a) cancel perfectly among themselves as z tends to 0, or to infinity. This occurs more rapidly than $K(z)$ tends towards its smallest value.

The new solution of Eq. (6) exhibits a more complex behaviour than the traditional ε^0 solution Eq. (3a). In addition to the exponentially decaying (first) parts in Eq. (6a), the second parts in Eq. (6a) go with the argument doubled (i.e. 2I(z)), which means a more rapid variation near the surface (as aloft this becomes negligible due to its exponential decay). Moreover, there are exponentially decaying terms in Eq. (6) that are not wave-like (the last parts). From Eq. (6) it is evident that the near-surface profiles of the final $\theta_{tot}(z)$ and $u_{tot}(z)$ in Eq. (2) are somewhat strengthened, and weakened, respectively; hence, the nonlinearity provides asymmetric effects on the meteorological fields (u,θ), as indicated by the different forcing in Eq. (5). This will immediately lead to a relatively larger near-surface Ri compared with that from the zero-order solution (e.g. Grisogono, 2003). Another remark on discussing Eq. (6) is that Smith (1977) found a qualitatively similar behaviour in his weakly nonlinear treatment of hydrostatic mountain waves steepening[‡]; there, the mountain waves were steeper on the lee side than on the windward side, thus allowing for wave asymmetry.

The total WKB solutions up to the first order are:

$$\begin{aligned}\theta_{\mathrm{tot,WKB}}(z)&=\theta_{0,\mathrm{WKB}}(z)+\varepsilon\theta_{1,\mathrm{WKB}}(z),\\u_{\mathrm{tot,WKB}}(z)&=u_{0,\mathrm{WKB}}(z)+\varepsilon u_{1,\mathrm{WKB}}(z).\end{aligned} \tag{7}$$

It cannot be overstressed that these results with gradually varying $K(z)$ are structurally the same as those for the $K=$ const case. Proceeding to the higher order terms, i.e., ε^2, ε^3, etc., would result in a set of coupled and progressively more complex ordinary differential equations for momentum and heat, with their corresponding forcing from the lower orders of power in ε. This is how the regular perturbation analysis works on a global level: a hard nonlinear problem is split into many simple problems, each bringing progressively less weight to the solution as the power of ε^n increases $(n\geq 0)$.

As the correction $u_{1,\mathrm{WKB}}(z)$ in Eq. (6) is mostly negative and proportional to $\sigma_0^{1/2}$, which also means proportional to the square root of the slope, i.e., $\sin^{1/2}(\alpha)$ (here the absolute value of α is taken), the total katabatic wind speed in Eq. (7), as well as its maximum, should decrease with increasing the slope angle α. This new analytic result is not contained in the classic Prandtl theory, where the katabatic speed maximum is insensitive to α. However, Grisogono and Axelsen (2012) found by using LES that the maximum katabatic speed should decrease with increasing slope angle (at least for the range $3^\circ\leq\alpha<6^\circ$, which they addressed explicitly); this decrease in the speed should be weaker than a linear trend, perhaps in a similar manner to the decrease of z_j with $\sin^{-1/2}(\alpha)$, which is also in agreement with our findings here (considering the range of slopes for which the Prandtl model is suitable). Hence, this study supports the experimental finding by Oerlemans and Grisogono (2002) and the LES finding by Grisogono and Axelsen (2012), which is, that z_j is largely proportional to the maximum katabatic wind speed, with correlation coefficients of 0.78 and 0.98, respectively. This also implies that both properties of the katabatic LLJ (i.e. the height and speed) should decrease for increasing slope α and vice versa (for the relatively small range of α considered, say, roughly, $0.5^\circ<\alpha<6^\circ$), although α as such could not be varied by Oerlemans and Grisogono (2002).

2.3. *Estimation of the small parameter ε*

What remains now is to estimate a suitable value of ε. As an appropriate value of ε should not depend on a particular method of solving differential equations (e.g. Bender and Orszag, 1978), we first plot katabatic profiles for the $K=$ const case together with Eq. (7) using various values of ε, with the knowledge that such profiles should not depart much from Eq. (3a) for our weakly nonlinear approach to be valid. Following that, we will augment our reasoning by a dynamical approach using external parameters of the model.

Figures 1 and 2 show typical katabatic profiles of (u,θ) using Eq. (2) up to the first order (or Eq. (7) but temporarily without invoking the WKB effects for simplicity). The zero-order solutions

[‡]There is not much similarity between the two studies, of course. Smith's treatment of weak nonlinearity goes through the lower BC and consequent steepening of the flow while the governing equation remains linear. In this study, it is the opposite: the lower BC remains fixed but the governing equation is expanded to include nonlinear terms.

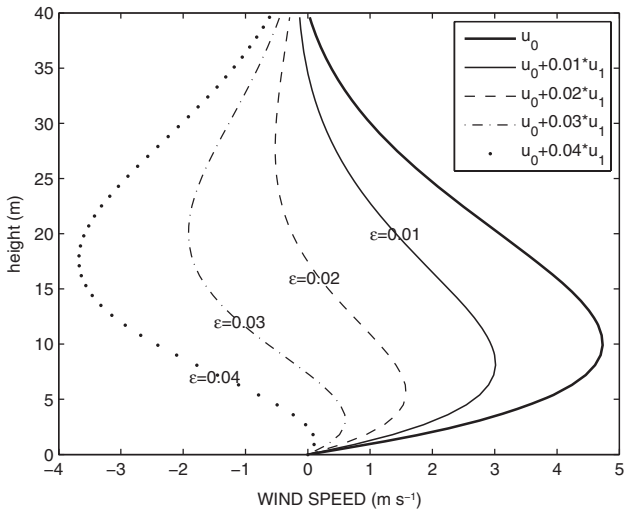

Figure 1. Katabatic wind-speed profiles using Eqs (2)–(7) and various values of the small parameter $\varepsilon = 0$, 0.01–0.04 are plotted. For simplicity, $K = \text{const} = 0.06\ \text{m}^2\ \text{s}^{-1}$; $Pr = 2$, $\alpha = -5^\circ$, $\Theta_0 = 273.14$ K, $\Gamma = 3\ \text{K km}^{-1}$, $C = -6^\circ$C (i.e. typical input parameters for the Prandtl model). Note that relatively larger values of ε cannot be related to a realistic katabatic flow.

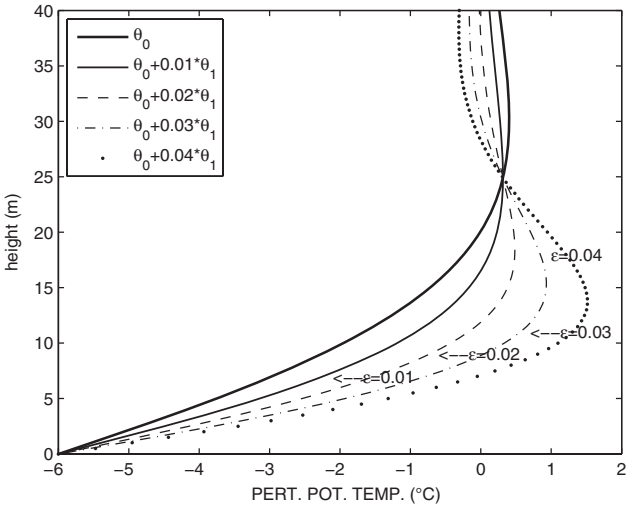

Figure 2. Same as Figure 1 but for typical katabatic potential temperature perturbation profile. The same reasoning regarding various ε profiles applies here as well.

are plotted as thick solid curves, while the corresponding profiles using various ε values are depicted as differently styled curves. As well as displaying typical katabatic flow profiles, the aim of these figures is to provide an estimate of a suitable value for the small parameter ε. Both figures strongly suggest that the upper limit for ε, in the context of simple katabatic flows, is 0.01. The profiles beyond $\varepsilon = 0.01$ should be disregarded because the weakly nonlinear effect becomes too large (the amplitude and the return flow of $u(z)$, and is comparable to the zero-order) if $\varepsilon > 0.01$, which is in contrast to the idea of the weak nonlinearity approach. Moreover, the near-surface inversion strength should not be roughly doubled, within the assumed weak nonlinearity, when compared with the zero-order solution (Figure 2, thick solid line, mostly lying to the left). Furthermore, the statically unstable layer above the bulk or the main part of the Prandtl flow (say, $z \geq 25$ m, in this case) should not be excessively unstable (e.g. $\text{d}\theta_{\text{tot}}/\text{d}z > -2\ \text{K}\,(100\ \text{m})^{-1}$), as for profiles using $\varepsilon > 0.01$. Thus, realistic katabatic flows should exist for the range of $0 \leq \varepsilon < 0.01$.

Furthermore, the expectations about the behaviour of a weakly nonlinear solution outlined below Eqs (5) and (6) are confirmed: compared with the classic Prandtl solution, the new solution exhibits weaker katabatic jets (Figure 1), occurring at lower heights and immersed in stronger stratification (Figure 2). Again, the first-order correction must really remain only a correction to the ε^0 solution.

The allowed range of ε values allowed may additionally be assessed by considering the total potential temperature gradient in Eq. (1). Since a weakly nonlinear model should not be able to alter the nature of a corresponding classic solution, by the same token, the total temperature gradient should not, on average, reverse its sign; thus, one may require from Eq. (1) that $\Gamma > \max(\varepsilon) \left| <\frac{\partial\theta_0}{\partial z}> \right|$, where $<\partial\theta_0/\partial z>$ is the average and the absolute value is taken to be on the safe side for both katabatic and anabatic flows. This absolute average is simply estimated to be $|<\frac{\partial\theta_0}{\partial z}>| = \frac{|C|}{2h_{\text{P}}}$, which is also in agreement with van den Broeke (1997a, 1997b), who used as katabatic flow forcing the bulk average of the surface potential temperature deficit, $C/2$. Hence,

$$\max(\varepsilon) < 2\Gamma h_{\text{P}}/|C|. \tag{8}$$

For typical katabatic flow input values in Eq. (8), say $\Gamma = 3\ \text{K km}^{-1}$, $h_{\text{P}} = 20$ m and $C = -6^\circ$C (all external parameters), $\max(\varepsilon) < 0.02$ is obtained. According to Eq. (8) and our previous reasoning related to Figures 1 and 2, it makes sense to retain our proposed and somewhat more stringent range for ε: $0 \leq \varepsilon < 0.01$ (see also section 3.1). Moreover, for simplicity, we shall choose the average value from the 'katabatic range', i.e., $\varepsilon = 0.005$. The dynamically based scaling argument for ε, involving Eq. (8), is necessary for a better understanding of the role and overall range of ε values that should be estimated from external parameters (in this case: α, C, Γ, g/Θ_0, K and Pr).

Note that in the case of anabatic flow the requirement Eq. (8) generally relates to the higher elevations than that for katabatic flow because, firstly, the surface is warmer than the adjacent air in anabatic flow so that θ first decreases with height, and secondly, an anabatic flow inversion is reached higher up, above h_{P} ($\sim K^{1/2}$) which is also a few times larger than that for katabatic flow. This immediately demands that ε for anabatic weakly nonlinear model should be a few or several times larger (see section 3.2) than that for katabatic flow.

2.4. *Choice of K(z) profile*

Gradually varying $K(z)$ may have an arbitrary yet slowly varying form, all within the validity of the WKB approach (e.g. GOa; GO2). Among the large class of $K(z)$ profiles allowed, we choose that of GOb, Jeričević and Večenaj (2009) and Jeričević *et al.* (2010):

$$K(z) = K_0 \frac{z}{h} \exp\left(-\frac{z^2}{2h^2}\right) + K_{\min}, \tag{9}$$

which depends on two parameters related to the maximum value of $K(z)$ and the elevation h where the maximum is attained, i.e., (K_0, h). Certain asymptotic properties related to Eq. (9) and the integral $I(z)$ are given in GOa, b; furthermore, extensive discussion, explanations and comparisons of this non-local first-order turbulence parametrization scheme with some other possible profiles are provided in the related references. Note from Eq. (9) that $\max(K(z)) = K_0 \exp(-1/2)$ is attained at $z = h$. To avoid a possible division by 0 when using Eq. (9), as in, e.g., Eq. (6b), a small constant amount of diffusivity is added to $K(z)$ in Eq. (9), $K_{\min}$, typically tenfold of that for molecular diffusivity of air (as in, e.g., Sun *et al.*, 2013; their eq. (25)).

3. Results and discussion

As the focus here, among the various possible slope flows, is on simple katabatic flow that is treated analytically, we proceed with this first.

3.1. *Simple katabatic flow*

Although the essence of a weakly nonlinear Prandtl model and its solutions is depicted in Figures 1 and 2, using $K = \text{const}$,

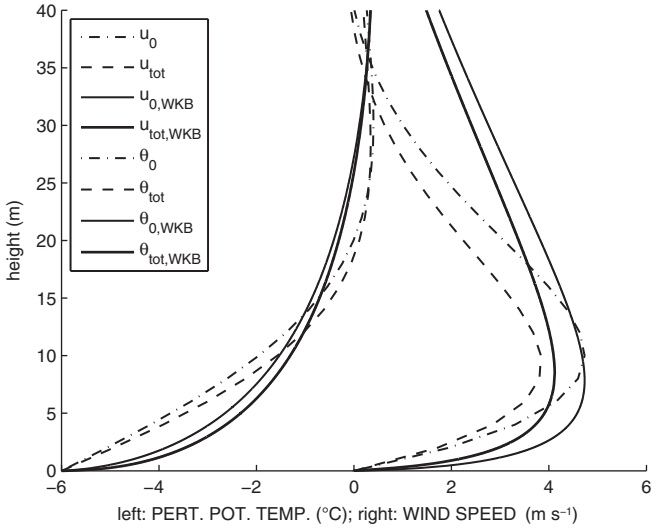

Figure 3. Katabatic wind speed (mostly on the right-hand side of the figure) and potential temperature perturbation (mostly on the left-hand side as deficit) profiles: classic linear, $(u,\theta)_0$, dot-dashed, and weakly nonlinear solution, $(u,\theta)_{\rm tot}$, dashed, using $\varepsilon = 0.005$ for $K =$ const and input parameters as in Figure 1; WKB linear, $(u,\theta)_{0,\rm WKB}$, thin solid, and WKB weakly nonlinear solution, $(u,\theta)_{\rm tot,WKB}$, thick solid, with $\varepsilon = 0.005$, for $K(z)$ from Eq. (9) with $\max(K(z)) = 0.3$ m^2 s^{-1} at $h = 30$ m, the other input parameters as in Figure 1 Subscript 0 and tot denote linear and total (i.e., weakly nonlinear) solutions, respectively.

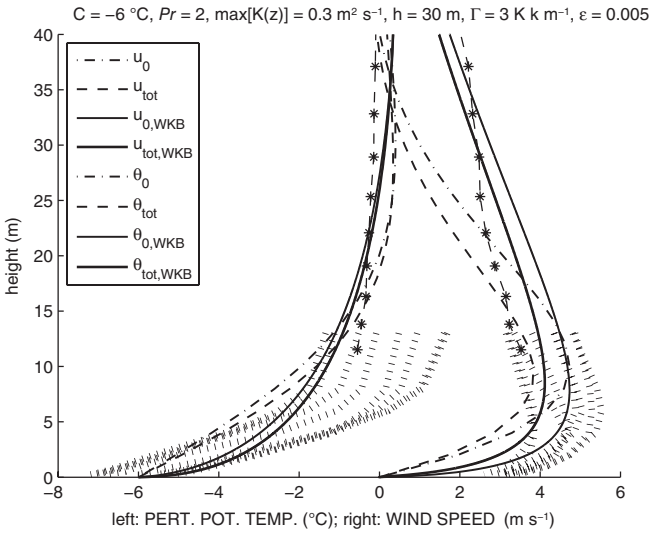

Figure 4. Data comparison for θ (potential temperature perturbation) and u (katabatic wind speed) among the WKB solutions ($u_{0,\rm WKB}$ – thin solid and, $u_{\rm tot,WKB}$ – thick solid, mostly on the RHS, $\theta_{0,\rm WKB}$ – thin solid and $\theta_{\rm tot,WKB}$ – thick solid, mostly on the left-hand side) versus two kinds of observations (eight-level tower data during 24 h, averaged over 3 h consecutively, light-hatched; balloon data at 1400 LST from the second highest tower level up, dash-asterisk) and the $K =$ const solutions (u_0 – dot-dashed, $u_{\rm tot}$ – dashed, θ_0 – dot-dashed, $\theta_{\rm tot}$ – dashed). The main input parameters are given above the profiles, slope $\alpha = -5^\circ$.

to emphasize the acceptable range of ε that controls the amount of nonlinearity, an additional comparison between this and the corresponding WKB solution follows. Figure 3 shows (i) the previously presented classic and the weakly nonlinear Prandtl solution for $K =$ const, and (ii) the corresponding WKB solutions, using $K(z)$ from Eq. (9), for both the classic and the weakly nonlinear solution. Among all solutions presented in Figure 3, the classic solution exhibits the weakest near-surface gradients of potential temperature and partly for wind speed, where the latter is comparable (for $z \leq 2$ m) to that for the nonlinear solution using $K =$ const. Furthermore, the classic solution for the wind-speed profiles decays more rapidly after reaching its maximum at the corresponding z_j, as previously established based on data from Defant (1949), Egger (1990) and GOa. The WKB solutions deliver sharper near-surface gradients, however, including a stronger inversion and a lower katabatic LLJ, which decreases more gradually after its maximum than in the classic solution. Regarding the weakly nonlinear solution, we focus now only on its WKB version, because the $K =$ const case has been discussed previously. This solution, shown by bold curves in Figure 3, exhibits the second sharpest wind-speed gradient with a moderately strong LLJ of ≈ 4 m s^{-1} (while the other solutions go up to almost 5 m s^{-1}), adjacent to the surface, all within the strongest near-surface temperature inversion of ≈ 5 K (10 m)$^{-1}$. Hence, the weakly nonlinear WKB solution describes the katabatic wind under the most stably stratified flow conditions.

Next, we compare the weakly nonlinear solution of Eqs (6) and (7) for katabatic flow using a suitable data set, which pertains to a glacier wind observed on the Pasterze glacier during the PASTEX-94 experiment (e.g. van den Broeke, 1997a, 1997b; GOa, b; Oerlemans and Grisogono, 2002). While GOa, b discussed and explained how and why the WKB solutions are better than the $K =$ const solutions, herein we concentrate on the further modifications of the WKB solutions using the weakly nonlinear approach developed. Figure 4 is organized in a similar manner as in GOb, their figure 3, in order to aid comparison, discussion and to stress the overall diurnal persistency of the glacier wind in spite of significant variations; details of the glacier wind diurnal variability are available in van den Broeke (1997a, 1997b). Although the observed glacier wind, as a nearly ideal katabatic flow, varies in its intensity throughout the 24 h period presented (eight-level tower data averaged over eight 3 h periods and a single balloon profile at 1400 LST (1200 UTC)), the prominent LLJ located around 5.5–7 m with a maximum speed of nearly 4 up to 5.8 m s^{-1} is always present. It is immersed into a strong near-surface inversion of about 6 to almost 8 K (13 m)$^{-1}$, that weakens significantly from about 8 to 15 m and upward. The weakly nonlinear WKB solution $u_{\rm tot,WKB}$ (bold solid curves in Figure 4), describes the overall, or the average data the best, even though the linear WKB solution $u_{0,\rm WKB}$ (thin solid curve) from GOb also remains very good, as the second best overall solution. In fact, solely from the tower data, which go up to 13 m above the glacier's surface, these two WKB solutions are of the same quality; however, the new solution, $u_{\rm tot,WKB}$, is closer to the balloon data aloft and thus appears to be the best. We substantiate this by calculating two statistical parameters, root mean square error (RMSE) and bias, between the profiles of each of the solutions and observations, both for the wind speed and potential temperature. Particularly, we calculate RMSE and bias by comparing the profile of a certain solution with the two profiles observed for the tower (the most suitable profiles for the comparison are those averaged between 0900 and 1200 LST and especially between 1200 and 1500 LST, following van den Broeke, 1997a) and that for the balloon ascent. According to the results shown in Table 1, $u_{0,\rm WKB}$ compares better with both tower profiles than $u_{\rm tot,WKB}$ does, which compares better with the balloon profile. Also, $\theta_{0,\rm WKB}$ is better than $\theta_{\rm tot,WKB}$ only for the earlier tower profile, whereas for the later one and for the balloon profile, $\theta_{\rm tot,WKB}$ is substantially better. To summarize, although for wind speed $u_{0,\rm WKB}$ is better than $u_{\rm tot,WKB}$ for the tower data, for temperature this is only partially true. On the other hand, for both wind speed and temperature, $u_{\rm tot,WKB}$ is better aloft with regard to the balloon data. Therefore, the verification in Table 1 favours the new solution $u_{\rm tot,WKB}$ slightly better.

We now discuss the data comparison versus the finest analytical solutions further by calculating and comparing the wind speed and temperature gradients using the observations and different solutions. Although the gradients obtained from $u_{0,\rm WKB}$ compare marginally better with those obtained from the tower observations, for the balloon data the corresponding gradients obtained from $u_{\rm tot,WKB}$ resemble the balloon gradients better (not shown). Hence, when compared with the limited data set and based on Figure 4 and Table 1, the new nonlinear solution

Table 1. Values of statistical parameters derived from the comparison of the tower and balloon profiles from PASTEX-94 with the profiles of different analytical solutions (the symbols as in Figure 4 and in the text). The units of RMSE and BIAS are m s^{-1} and K for wind speed and potential temperature, respectively.

Measurement location	Error and bias	u_0	u_{tot}	$u_{0,WKB}$	$u_{tot,WKB}$	θ_0	θ_{tot}	$\theta_{0,WKB}$	$\theta_{tot,WKB}$
Tower 0900–1200 LST	RMSE	2.10	2.19	1.05	1.43	1.37	1.16	1.22	1.36
	Bias	−1.39	−1.80	−0.39	−1.03	−0.67	−0.48	0.13	0.46
Tower 1200–1500 LST	RMSE	1.82	1.81	1.01	1.15	2.08	1.85	1.36	1.17
	Bias	−0.91	−1.32	0.09	−0.55	−1.83	−1.64	−1.03	−0.70
Balloon 1400 LST	RMSE	1.18	1.25	0.85	0.48	0.53	0.42	0.39	0.32
	Bias	−0.25	−0.90	0.71	0.29	0.11	0.21	−0.09	0.00

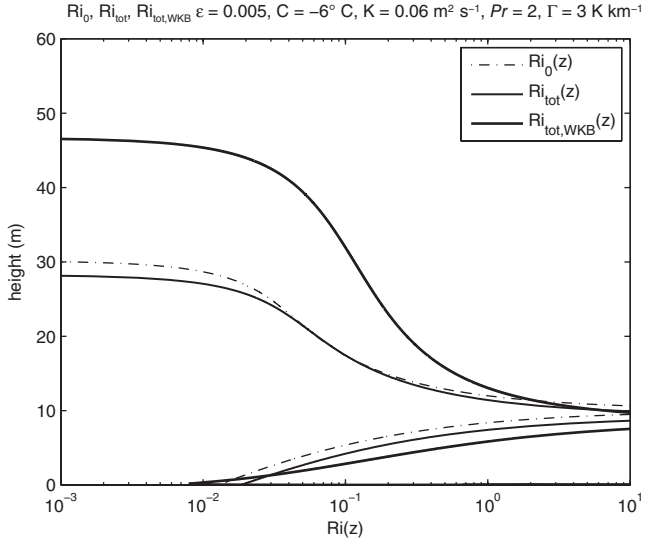

Figure 5. Semi-logarithmic plot of the gradient Richardson number $Ri(z)$ profiles for $K = \text{const}$ (= 0.06 m^2 s^{-1} as before) using classic linear (dot-dashed) and weakly nonlinear (thin solid), and the weakly nonlinear (thick solid) Prandtl model with $K(z)$ using Eq. (9); max($K(z)$) = 0.3 m^2 s^{-1}at $h = 30$ m. The other input parameters as before.

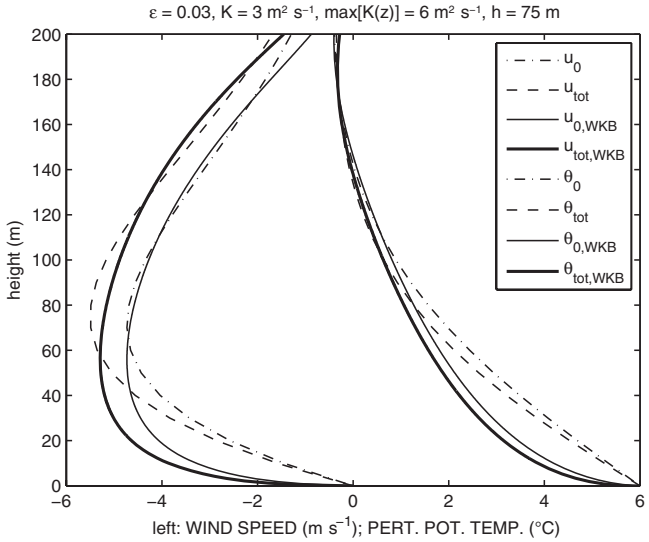

Figure 6. Anabatic wind speed (on the left-hand side) and potential temperature perturbation (on the right-hand side) profiles. Symbols and curves as in Figure 3: classic linear, $(u, \theta)_0$, dot-dashed, and weakly nonlinear solution, $(u, \theta)_{tot}$, dashed, using $\varepsilon = 0.03$ for $K = \text{const} = 3$ m^2 s^{-1}; WKB linear, $(u, \theta)_{0,WKB}$, thin solid, and WKB weakly nonlinear solution, $(u, \theta)_{tot,WKB}$, thick solid, with $\varepsilon = 0.03$, for $K(z)$ from Eq. (9) with max($K(z)$) = 6 m^2 s^{-1} at $h = 75$ m; other input parameters as in Figure 1 except that now $C = +6°$C.

presented here appears to be marginally better than the linear WKB solution from GOa, b.

It is seen in both Figures 3 and 4 that the weakly nonlinear solution, when compared with the previous solutions, represent the stronger near-surface stratification and somewhat weaker katabatic LLJ. Another way to see the corresponding dynamical effect of stratification and wind shear is to plot $Ri(z)$ as depicted in Figure 5, in which the LLJ in the new weakly nonlinear solution is generally the lowest and thickest when compared to other solutions.

To avoid tedious, though straightforward, analytic calculations using three Prandtl solutions for the three $Ri(z)$ presented in Figure 5, each $Ri(z)$ is calculated numerically at a very fine vertical resolution. Two different numerical methods using finite differences are used; excellent agreement is obtained except at the uppermost grid-point where the methods vary by a factor of two, but this point (above 100 m) is irrelevant for our analysis. The simplest among Ri(z), i.e., $Ri_0(z)$, is also checked analytically. At the same time, all $Ri(z)$ versions addressed have the same overall structure, which can be summarized as:

$$Ri(z) = -\frac{gh_P}{\Theta_0 C\mu^2}\exp(F_1(z))\,F_2(z), \qquad (10)$$

with various levels of complexity. In the simplest case of $Ri_0(z)$, $F_1 = z/h_P$ and $F_2 = [\cos(z/h_P) + \sin(z/h_P)]/[\sin(z/h_P) - \cos(z/h_P)]^2$; otherwise, F_1 and F_2 become lengthy expressions involving ratios of derivatives of Eq. (6) that also contain trigonometric functions of the integral $I(z)$ used in Eq. (3b).

Compared with the classic solution, the weakly nonlinear Prandtl solution of Eqs (6) and (7) yields, via Eq. (10), a lowered z_j and the corresponding height where $Ri \to \infty$, Figure 5. For $z < 2$ m this new solution, for the typical input given, represents the lowest dynamic stability with $Ri \leq 0.02$. Above that lowest sublayer $\sim O(2$ m), throughout the most of katabatic flow, the new solution exhibits the largest Ri values, which may enhance the possibility for flow decoupling from the upper layers via the Scorer parameter consideration (Parmhed *et al.*, 2004; Mahrt, 2014); this, in turn, may modify the turbulent fluxes over glaciers and their mass balance (e.g. Munro, 2004). Overall, the new solution also implies the thickest strongly stratified SABL (where the Prandtl layer is its lower part) among all the solutions considered.

3.2. *Simple anabatic flow*

Next, we briefly address a simple anabatic flow for which the same weakly nonlinear approach developed here also may be applied. For simplicity and consistency, we retain as many input parameters as possible (see Figures 3–5). However, now $C > 0$, as a surface potential temperature surplus, thus the K value also must be enlarged and consequently h_P; therefore, this demands a larger ε than that for katabatic flows (see section 2.3). Figure 6 displays typical anabatic flow profiles.

From Figure 6 it appears that the potential temperature of anabatic flow decreases more rapidly with height when using the weakly nonlinear solution and/or WKB method. Furthermore, in the same solutions the corresponding anabatic wind (plotted as negative values, in order to contrast with the katabatic wind, which blows in the opposite direction) increases with height more rapidly, reaching its maximum at lower elevations. There are two effects present in the $\theta_{tot,WKB}$ rapid decrease and $u_{tot,WKB}$ rapid increase with height: near-surface mixing reduction due to

a locally smaller $K(z)$, compared with that for $K = \text{const}$ and the weakly nonlinear feedback. Between these two effects, there is a stronger effect of the $K(z)$ near-surface mixing reduction on the temperature profile for, roughly $z \leq 80$ m (for $z > 80$ m the weakly nonlinear feedback dominates but the overall effect is already very small). However, for the wind speed both effects appear as equally important. Namely, for the anabatic wind speed the effect of reduction of $K(z)$ is stronger for $z < 40$ m, while the weakly nonlinear effect is stronger for $z > 45$ m.

The linear solutions produce about 15 to even 20% weaker anabatic LLJ than the weakly nonlinear solutions (two leftmost profiles in Figure 6). In particular, the classic solution $u_0(z)$ and the new weakly nonlinear solution using $K(z)$, i.e., $u_{\text{tot,WKB}}$, when integrated through 200 m depth (Figure 6), give the mean anabatic wind speeds of 3.25 and 4.14 m s^{-1} (the latter is more than 20% higher than the former), respectively. Hence, unlike in the katabatic flow, here the new solutions result in a LLJ enhancement in a more statically unstable ABL than that in the classic Prandtl solution for anabatic flow. This might have certain positive consequences on straightforward wind-energy potential estimates (the yield goes with the mean wind speed cubed, e.g., Horvath *et al.*, 2011) because going from, e.g., 4 to 5 m s^{-1} in the mean wind speed, allows for about a doubling in the wind-power potential. Moreover, daytime valley ventilation via anabatic flows appears now to be more intensive, while its night-time katabatic counterpart becomes weaker, when both are compared with the classic Prandtl solution. This finding agrees qualitatively with the finding by Nadeau *et al.* (2013) that the night-time downslope and downvalley winds are lighter than the daytime thermally driven upslope and upvalley flows.

3.3. *Summary on simple slope flows*

Two combined effects appear important for details of simple slope flows: nonlinearity and variable diffusivity $K(z)$. To sum up, the weakly nonlinear solution of Eqs (6) and (7) up to the ε^1 term using $K(z)$, produces sharper temperature perturbations, i.e., steeper vertical gradients, in both katabatic and anabatic flows. The enhanced advection of θ via the $\varepsilon \partial\theta/\partial z$ term, yielding lowest θ values near the surface, is (mildly) balanced near the surface where the $K(z)$ values are low (and the corresponding parametrized turbulent eddies are thus very small), which allows for an enhanced total vertical temperature gradient near the surface. As the former relates to the relatively thin, strongly stratified SABL with significantly reduced turbulent (parametrized here) mixing, except in the lowest few metres where also strong wind shear dominates and thus $0 < Ri \leq 0.1$, the katabatic LLJ becomes generally reduced when compared with that based on the linear solution, which is of the ε^0 order (without or with the WKB modification for $K(z)$). Namely, in the linear Prandtl solution the established strong stratification, via dominant temperature perturbation, does not feed back to the dynamics of katabatic flow. It is shown that the nonlinearity affects the elevation and strength of the LLJ in simple slope flows. For simple anabatic flow occurring in the convective ABL, more vigorous mixing appears (a more rapid temperature decrease with height in our weakly nonlinear Prandtl model) and thus, a more intensive anabatic LLJ forms than that obtained from the linear Prandtl solution.

All those points could account for an improvement in the turbulence parametrizations, including thermally driven slope flows in NWP and climate models (e.g. Barthélemy *et al.*, 2012). Namely, for a given dominant slope angle $\alpha(x, y)$, surface potential temperature perturbation, background stratification and a current state of eddy diffusivity, a near-surface u and θ can be estimated, as well as the corresponding vertical fluxes, and fed back to the model. The information can then be used in various applications ranging from glacier mass-balance estimation, pragmatic meteorological modelling (e.g. affecting the Obukhov length, Grisogono *et al.*, 2007), to wind-energy harvesting (e.g. Horvath *et al.*, 2011), etc. We leave those avenues for future work.

4. Conclusions

Slope flows occupy the focus of geophysical fluid research for many reasons (Renfrew and Anderson, 2002, 2006; Shapiro *et al.*, 2012; Chow *et al.*, 2013). Simple slope flows are addressed herein by the extension and evaluation of analytic models based on the classic work of Prandtl. Our modification of the Prandtl model, making it weakly nonlinear, is somewhat similar to the analytic treatment of sea-breeze nonlinearity by Gutman (1972). The emphasis here is on a type of very stratified SABL, dealing with inclined cooled surfaces, i.e., simple katabatic flows, although the opposite flow (i.e. common anabatic wind) is tackled as well. For this purpose, a regular perturbation analysis is deployed.

As slope flows in an undisturbed, quiescent atmosphere are primarily thermally driven, the goal of this study was to seek an explicit nonlinear response of the flow to the temperature perturbation. Namely, flow-induced potential temperature gradient is allowed to feed back to the overall (environmental) potential temperature gradient because the former (by absolute values) can be 20–50 times stronger than the latter (e.g. GOa; Oerlemans, 2001). That fact has significant consequences on the slope flow, as shown in this work, in which the weakly nonlinear Prandtl model is developed and explored. A better (physically more consistent) solution has been presented when compared with the classic Prandtl model. The new results lead to a qualitatively similar modification in height and strength of the LLJ as that produced by the linear WKB approach with gradually varying eddy diffusivity and conductivity $K(z)$.

One of the main points from this study is that the purely linear Prandtl solution (of the order of ε^0, where ε is the small parameter in the regular perturbation expansion) produces weaker near-surface stratification with a stronger katabatic wind than that obtained here by using the weakly nonlinear Prandtl model up to the ε^1 order of the solution expansion. This occurs with both $K = \text{const}$ and WKB solutions using gradually varying $K(z)$, and both pertain to the new, weakly nonlinear solution. A limited data comparison confirms this finding, although within the uncertainty inherent in a limited data set the weakly nonlinear improvement of the model is not very significant when compared with the linear WKB model. The estimated optimum value of ε is 0.005 and 0.03 for katabatic and anabatic flow, respectively. Moreover, this study shows that the maximum katabatic wind speed should decrease with increasing underlying slope angle α, a result found in both the limited data set and for LES (Oerlemans and Grisogono, 2002; Grisogono and Axelsen, 2012), but a feature that is not contained in the linear Prandtl theory.

The (weak) nonlinearity affects the elevation and strength of the LLJ in both the katabatic and anabatic cases, which, in turn, inevitably modifies the dynamic stability of the layers below and above the LLJ. Furthermore, based on the thermally driven nonlinearity in the Prandtl slope-flow theory considered in this work, anabatic winds are more enhanced whereas katabatic winds become weakened, when compared with their respective counterparts from linear theory.

Finally, we discussed some of the consequences of the analytical approach deployed here, speculated on further applications and summarized the main steps of the article. From a broader perspective, this analytical study can be useful for parametrizing inclined boundary layers in NWP and climate models, as well as in improving calculations of wind over glaciers (important for glacier mass balance and other microclimate-related issues) and wind-energy potential over mountainous terrain. In other words, the new solution may be used as a basis for a parametrization of unresolved simple slope flows in NWP and climate models.

Acknowledgements

The Reviewers are thanked for numerous improvements to the original manuscript and its overall readability. This study is supported by the Croatian Ministry of Science, Education and Sports (MZOS), project BORA No. 119-1193086-1311, and the Croatian Science Foundation, project CATURBO, No. 09/151. I.G. is supported by the MZOS project No. 004-1193086-3035.

References

Axelsen SL, van Dop H. 2009a. Large-eddy simulation of katabatic wind. Part I: Comparison with observations. *Acta Geophys.* **57**: 803–836, doi: 10.2478/s11600-009-0041-6.

Axelsen SL, van Dop H. 2009b. Large-eddy simulation of katabatic wind. Part II: Sensitivity study and comparison with analytic models. *Acta Geophys.* **57**: 837–856, doi: 10.2478/s11600-009-0042-5.

Baklanov A, Grisogono B, Bornstein R, Mahrt L, Zilitinkevich S, Taylor P, Larsen S, Rotach M, Fernando HJS. 2011. The nature, theory and modeling of atmospheric planetary boundary layers. *Bull. Am. Meteorol. Soc.* **92**: 123–128.

Barthélemy A, Goosse H, Mathiot P, Fichefet T. 2012. Inclusion of a katabatic wind correction in a coarse-resolution global coupled climate model. *Ocean Modell.* **48**: 45–54.

Belušić D, Güttler I. 2010. Can mesoscale models reproduce meandering motions? *Q. J. R. Meteorol. Soc.* **136**: 553–565.

Belušić D, Mahrt L. 2008. Estimation of length scale from mesoscale networks. *Tellus* **60A**: 706–715.

Bender CM, Orszag SA. 1978. *Advanced Mathematical Methods for Scientists and Engineers.* McGraw-Hill Inc: New York, NY.

Berger BW, Grisogono B. 1998. The baroclinic, variable eddy viscosity Ekman layer. An approximate analytical solution. *Boundary Layer Meteorol.* **87**: 363–380.

van den Broeke MR. 1997a. Structure and diurnal variation of the atmospheric boundary layer over a mid-latitude glacier in summer. *Boundary Layer Meteorol.* **83**: 183–205.

van den Broeke MR. 1997b. Momentum, heat and moisture budgets of the katabatic wind layer over a mid-latitude glacier in summer. *J. Appl. Meteorol.* **36**: 763–774.

van den Broeke MR, van Lipzig NPM. 2003. Factors controlling the near-surface wind field in Antarctica. *Mon. Weather Rev.* **131**: 733–743.

Burkholder BA, Shapiro A, Fedorovich E. 2009. Katabatic flow induced by a cross-slope band of surface cooling. *Acta Geophys.* **57**: 923–949, doi: 10.2478/s11600-009-0025-6.

Buzzi M, Rotach MW, Raschendorfer M, Holtslag AAM. 2011. Evaluation of the COSMO-SC turbulence scheme in a shear-driven stable boundary layer. *Meteorol. Z.* **20**: 335–350.

Chow FK, de Wekker SFJ, Snyder BJ (eds.). 2013. *Mountain Weather Research and Forecasting.* Springer: Dordrecht, Netherlands.

Defant F. 1949. Zur theorie der Hangwinde, nebst bemerkungen zur Theorie der Berg- und Talwinde. *Arch. Meteorol. Geophys. Bioklimatol. Ser. A* **1**: 421–450, doi: 10.1007/BF02247634.

Denby B. 1999. Second-order modelling of turbulence in katabatic flows. *Boundary Layer Meteorol.* **92**: 67–100.

Egger J. 1990. Thermally forced flows: Theory. *Atmospheric Processes Over Complex Terrain:* 43–57. American Meteorological Society: Boston, MA.

Epifanio CC. 2007. A method for imposing surface stress and heat flux conditions in finite-difference models with steep terrain. *Mon. Weather Rev.* **135**: 906–917.

Fedorovich E, Shapiro A. 2009. Structure of numerically simulated katabatic and anabatic flows along steep slopes. *Acta Geophys.* **57**: 981–1010, doi: 10.2478/s11600-009-0027-4.

Grisogono B. 2003. Post-onset behaviour of the pure katabatic flow. *Boundary Layer Meteorol.* **107**: 157–175.

Grisogono B. 2010. Generalizing "z-less" mixing length for stable boundary layers. *Q. J. R. Meteorol. Soc.* **136**: 213–221.

Grisogono B, Axelsen SL. 2012. A note on the pure katabatic wind maximum over gentle slopes. *Boundary Layer Meteorol.* **145**: 527–538.

Grisogono B, Belušić D. 2009. A review of recent advances in understanding the meso- and micro-scale properties of the severe Bora wind. *Tellus* **61A**: 1–16.

Grisogono B, Oerlemans J. 2001a. A theory for the estimation of surface fluxes in simple katabatic flows. *Q. J. R. Meteorol. Soc.* **127**: 2725–2739 (referred to as GOa).

Grisogono B, Oerlemans J. 2001b. Katabatic flow: Analytic solution for gradually varying eddy diffusivities. *J. Atmos. Sci.* **58**: 3349–3354 (referred to as GOb).

Grisogono B, Oerlemans J. 2002. Justifying the WKB approximation in pure katabatic flows. *Tellus* **54A**: 453–463 (referred to as GO2).

Grisogono B, Kraljević L, Jeričević A. 2007. The low-level katabatic jet height versus Monin–Obukhov height. *Q. J. R. Meteorol. Soc.* **133**: 2133–2136.

Gutman LN. 1972. *Introduction to the Nonlinear Theory of Mesoscale Meteorological Processes*, Gidrometeorologicheskoe Izdatel'stvo, Leningrad. Keter Press: Jeruzalem.

Haiden T. 2003. On the pressure field in the slope wind layer. *J. Atmos. Sci.* **60**: 1632–1635.

Horvath K, Bajić A, Ivatek-Šahdan S. 2011. Dynamical downscaling of wind speed in complex terrain prone to bora-type flows. *J. Appl. Meteorol. Climatol.* **50**: 1676–1691.

Jeričević A, Večenaj Ž. 2009. Improvement of vertical diffusion analytic schemes under stable atmospheric conditions. *Boundary. Layer Meteorol.* **131**: 293–307.

Jeričević A, Kraljević L, Grisogono B, Fagerli H, Večenaj Ž. 2010. Parameterization of vertical diffusion and the atmospheric boundary layer height determination in the EMEP model. *Atmos. Chem. Phys.* **10**: 341–364.

Jeričević A, Fagerli H, Grisogono B. 2012. Exploring the properties of local and non-local vertical diffusion schemes in the EMEP model using 222Rn data. *Int. J. Environ. Pollut.* **48**: 231–243.

Jurlina T. 2013. *Weakly Non-Linear Modification of the Prandtl Model for Katabatic Flow*, Diploma Work. Department of Geophysics, Faculty of Science, University of Zagreb (In Croatian[§]), http://bib.irb.hr/prikazi-rad?&rad=628482 (accessed 10 October 2013).

Kavčič I, Grisogono B. 2007. Katabatic flow with Coriolis effect and gradually varying eddy diffusivity. *Boundary Layer Meteorol.* **125**: 377–387.

Lykosov VN, Gutman LN. 1972. Turbulent boundary layer above a sloping underlying surface. *Izv. Atmos. Oceanic Phys.* **8**: 462–467.

Mahrt L. 1982. Momentum balance of gravity flows. *J. Atmos. Sci.* **39**: 2701–2711.

Mahrt L. 1998. Stratified atmospheric boundary layers and breakdown of models. *Theor. Comput. Fluid Dyn.* **11**: 263–279.

Mahrt L. 2008a. Bulk formulation of the surface fluxes extended to weak-wind stable conditions. *Q. J. R. Meteorol. Soc.* **134**: 1–10.

Mahrt L. 2008b. Mesoscale wind direction shifts in the stable boundary-layer. *Tellus* **60A**: 700–705.

Mahrt L. 2014. Stably stratified atmospheric boundary layers. *Annu. Rev. Fluid Mech.* **46**: 23–45.

Mo R. 2013. On adding thermodynamic damping mechanisms to refine two classical models of katabatic winds. *J. Atmos. Sci.* **70**: 2325–2334.

Mauritsen T, Svensson G, Zilitinkevich S, Esau I, Enger L, Grisogono B. 2007. A total turbulent energy closure model for neutral and stably stratified atmospheric boundary layers. *J. Atmos. Sci.* **64**: 4113–4126.

Munro DS. 2004. Revisiting bulk heat transfer on Peyto Glacier, Alberta, Canada, in light of the CIG parameterization. *J. Glaciol.* **50**: 590–600.

Nadeau DF, Pardyjak ER, Higgins CW, Parlange MB. 2013. Similarity scaling over a steep Alpine slope. *Boundary Layer Meteorol.* **147**: 401–419.

Nappo CJ, Rao KS. 1987. A model study of pure katabatic flow. *Tellus* **39A**: 61–71.

Nikulin G, Kjellström E, Hansson U, Strandberg G, Ullerstig A. 2011. Evaluation and future projections of temperature, precipitation and wind extremes over Europe in an ensemble of regional climate models. *Tellus* **63A**: 41–55.

Oerlemans J. 2001. *Glaciers and Climate Change.* Balkema Publishers: Lisse, Netherlands.

Oerlemans J, Grisogono B. 2002. Glacier wind and parameterization of the related surface heat flux. *Tellus* **54A**: 440–452.

Oerlemans J, Vugts HF. 1993. A meteorological experiment in the melting zone of the Greenland ice sheet. *Bull. Am. Meteorol. Soc.* **74**: 355–365.

Oerlemans J, Björnsson H, Kuhn M, Obleitner F, Palsson F, Smeets P, Vugts HF, de Wolde J. 1999. A glacio-meteorological experiment on Vatnajökull, Iceland, Summer 1996. *Boundary Layer Meteorol.* **92**: 3–26.

Parmhed O, Oerlemans J, Grisogono B. 2004. Describing surface-fluxes in katabatic flow on Breidamerkurjökull, Iceland. *Q. J. R. Meteorol. Soc.* **130**: 1137–1151.

Pedlosky J. 1987. *Geophysical Fluid Dynamics* (2nd edn). Springer-Verlag: New York, NY.

Pielke RA. 1984. *Mesoscale Numerical Modeling.* Academic Press: New York, NY.

Prandtl L. 1942. *Führer durch die Strömungslehre.* Vieweg und Sohn: Braunschweig, Germany.

Princevac M, Fernando HJS. 2007. A criterion for the generation of turbulent anabatic flows. *Phys. Fluids* **19**: 105102–105107, doi: 10.1063/1.2775932.

Renfrew IA, Anderson PS. 2002. The surface climatology of an ordinary katabatic wind regime in Coats Land, Antarctica. *Tellus* **54A**: 463–484.

Renfrew IA, Anderson PS. 2006. Profiles of katabatic flow in summer and winter over Coats Land, Antarctica. *Q. J. R. Meteorol. Soc.* **132**: 779–882.

Rotach M, Zardi D. 2007. On the boundary-layer structure over highly complex terrain: Key findings from MAP. *Q. J. R. Meteorol. Soc.* **133**: 937–948.

Shapiro A, Burkholder B, Fedorovich E. 2012. Analytical and numerical investigation of two-dimensional katabatic flow resulting from local surface cooling. *Boundary Layer Meteorol.* **145**: 249–272.

[§]The authors are willing to provide to the reader an English translation or interpretation of any particular fraction of this diploma work (the latter can be downloaded from the website).

Smeets CJPP, Duynkerke PG, Vugts HF. 1999. Observed wind profiles and turbulence fluxes over an ice surface with changing surface roughness. *Boundary Layer Meteorol.* **92**: 101–123.

Smith RB. 1977. The steepening of hydrostatic mountain waves. *J. Atmos. Sci.* **34**: 1634–1654.

Smith RB. 1979. The influence of mountains on the atmosphere. *Adv. Geophys.* **21**: 87–230, doi: 10.1016/S0065-2687(08)60262-9.

Smith RB. 1987. Aerial observations of the Yugoslavian Bora. *J. Atmos. Sci.* **44**: 269–297.

Smith CM, Skyllingstad ED. 2005. Numerical simulation of katabatic flow with changing slope angle. *Mon. Weather Rev.* **133**: 3065–3080.

Stiperski I, Kavčič I, Grisogono B, Durran DR. 2007. Including Coriolis effects in the Prandtl model for katabatic flow. *Q. J. R. Meteorol. Soc.* **133**: 101–106.

Sun J, Lenshow DH, Mahrt L, Nappo C. 2013. The relationships among wind, horizontal pressure gradient, and turbulent momentum transport during CASES-99. *J. Atmos. Sci.* **70**: 3397–3414.

Svensson G, Holtslag AAM. 2009. Analysis of model results for the turning of the wind and related momentum fluxes in the stable boundary layer. *Boundary Layer Meteorol.* **132**: 261–277.

Van der Avoird E, Duynkerke PG. 1999. Turbulence in a katabatic flow. Does it resemble turbulence in stable boundary layers over flat surfaces? *Boundary Layer Meteorol.* **92**: 39–66.

Van de Wiel BJH, Moene AF, Steeneveld GJ, Hartogensis OK, Holtslag AAM. 2007. Predicting the collapse of turbulence in stably stratified boundary layers. *Flow Turbul. Combust.* **79**: 251–274.

Zardi D, Whiteman CD. 2013. Diurnal mountain wind systems. In *Mountain Weather Research and Forecasting*, Chow FK, de Wekker SFJ, Snyder BJ. (eds.): 35–119 (750 pp.). Springer: Dordrecht, Netherlands.

Zilitinkevich SS, Elperin T, Kleeorin N, Rogachevskii I, Esau I, Mauritsen T, Miles MW. 2008. Turbulence energetics in stably stratified geophysical flows: Strong and weak mixing regimes. *Q. J. R. Meteorol. Soc.* **134**: 793–799.

